

## Creep and shrinkage effects in service stresses of concrete cable-stayed bridges

Jose Antonio Lozano-Galant<sup>\*1a</sup> and Jose Turmo<sup>2b</sup>

<sup>1</sup>*Department of Civil Engineering, University of Castilla-La Mancha, Spain*

<sup>2</sup>*Department of Construction Engineering, Universitat Politècnica de Catalunya, BarcelonaTech, Spain*

(Received September 18, 2013, Revised January 15, 2014, Accepted January 21, 2014)

**Abstract.** Most of the methods presented in the literature to define the target service stresses (Objective Service Stage, OSS) of cable-stayed bridges rarely include the time-dependent phenomena effects. Nevertheless, especially in concrete structures, this assumption might be on the unsafe side because time-dependent phenomena usually modify service stresses. To fill this gap, this paper studies the time-dependent phenomena effects into service stresses of concrete cable-stayed bridges. After illustrating the important role of these phenomena in an asymmetrical cable-stayed bridge without backstay, a new method to include their effects into the OSS is presented. An important issue to be considered in this method is the target time in which the OSS is defined to be achieved. The application of this method to two different structures showed the convenience of defining the OSS to be achieved at early times because that way the envelope of service stresses is reduced.

**Keywords:** cable-stayed bridge; time-dependent phenomena; creep; shrinkage; concrete; service stresses

### 1. Introduction

One of the first stages in the design of the construction process of a cable-stayed bridge is the definition of a target geometry and/or stress state to be achieved in service. This stage is known as the Objective Service Stage (OSS). In this stage, a given load hypothesis is counterbalanced by several resistant mechanisms. All these resistant mechanisms are related, to a greater or lesser extent, with the tensile forces of the stay cables. Since modern cable-stayed bridges are highly statically redundant structures, there does not exist a unique solution for calculating the stay cable forces in the OSS. The prestressing forces in stays represent a design parameter that can be tailored to achieve an effective design for the bridge. However, as the number of the stay cables increases, the evaluation of the proper set of stay cable forces in service becomes a challenging exercise.

Many of the criteria proposed in the literature to estimate the stay forces in the OSS have been reviewed in the literature (see Guan 2000, Chen *et al.* 2000, Hassan *et al.* 2012, Lozano-Galant *et al.* 2012a, b). According to these authors, the main criteria are as follows: (1) The Pendulus Rule (see SETRA 2001). The pendulus rule is a simplified criterion usually applied by the designers as a

---

\*Corresponding author, Ph.D., E-mail: joseantonio.lozano@uclm.es

<sup>a</sup>Ph.D. E-mail: jose.turmo@upc.edu

first approximation of the stay cable forces in the *OSS* in nearly horizontal decks. (2) Minimal Bending Energy Criterion (see Du 1989). As its name states, this criterion is based on the minimization of the bending energy of the structure. (3) Rigidly Supported Continuous Beam Criterion (see Chen *et al.* 2000, and Gimsing 1997). This criterion assumes that the long-term behavior of a cable-stayed bridge corresponds with that of an equivalent continuous beam. This beam is defined by removing the stay cables and adding fictitious bearings at the connections between the bridge deck and the stay cables. In this way, the tensile forces in the stay cables are obtained by projecting the vertical reactions of the corresponding fictitious supports into the stay cable directions. (4) Zero Displacement Criterion (see Lazar *et al.* 1972 and Wang *et al.* 1993). This criterion defines the stay cable forces to achieve zero deflections at certain control points of the structure. A common criterion consists of defining zero vertical deflection at the deck-stay connection and zero horizontal deflection at the top of the pylon in structures with backstays. Hassan *et al.* (2012) and Hassan (2013) introduced B-spline curves to analyze the bridge deflections. In these works, genetic algorithms were introduced to define the post-tensioning functions that minimized the deck deflections. (5) The Unit Load Method (see Janjic *et al.* 2002, 2003). This criterion is based on a linear system of equations that includes a degree of freedom for each stay cable force. This system relates the bending moments at some control points for two types of load cases: unit prestressing loads at each stay cable and the target load of the superstructure. (6) Optimization Criterion (see Negrao and Simoes 1997 and Simoes and Negrao 2000). In this criterion the prestressing stay cable forces are defined by the minimization of a scalar objective function. Different tendencies are used to define these objective functions. Some designers base their objective functions on the structural efficiency while some other base it on the economy of the structure.

Many researches (see e.g. Fiore *et al.* 2012 and Gogic and Sadovic 2012) have stated the important role that the time-dependent phenomena might play in the structural behavior of prestressed structures. In the case of cable-stayed bridges these effects make that the service stress state varies with time, and therefore, the *OSS* can only be obtained at a certain Target Time,  $t_T$ . Some works have been presented in the literature to study the time-dependent phenomena effects in stayed structures. Scotti (2003) defined the stay forces to minimize the creep effects throughout time in cable-stayed bridges with vertical stays. Giussani *et al.* (2004) analyzed the evolution of stresses and deformations of cable-stayed bridges over time. Martins *et al.* (2011) proposed a procedure to determine stay forces using an optimization algorithm that included the effects of time-dependent phenomena and staggered erection on cantilever. This method enables to define the stay forces to correct errors during erection stages. Nevertheless, as far as the authors know, the time-dependent phenomena effects are rarely included into the definition of the *OSS* of cable-stayed bridges. In addition to this, the effects of the creep and shrinkage in asymmetrical concrete cable-stayed bridges without backstays (such as the Alamillo Bridge) have not been conveniently reported in the literature.

To fill these gaps, the aim of this paper is to study the effects of time-dependent phenomena (creep and shrinkage) into the *OSS* of concrete cable-stayed bridges. To do so, a new method is proposed to include the effects of those phenomena into the *OSS*. This method is applied to an asymmetrical cable-stayed bridge without backstay and to a real cable-stayed bridge.

This paper is organized as follows: Section 2 deals with the time-dependent phenomena effects in service. In Section 3, a new method to include the time-dependent phenomena effects into service stresses is presented. In Section 4, this method is applied to study different  $t_T$  in two cable-stayed bridges. Finally, some conclusions are presented in Section 5.

## 2. Time-dependent phenomena effects in service

In this section a procedure to simulate time-dependent phenomena effects is first described. Then, a method presented in the literature to calculate the service stresses of cable-stayed bridges without taking into account the time-dependent phenomena effects is presented. Finally, a parametric analysis is presented to illustrate the important role that time-dependent phenomena play in singular cable-stayed bridges. This example (Example 1) shows the necessity of developing new methods to include the time-dependent phenomena effects into the definition of the OSS.

### 2.1 Time-dependent phenomena simulation

The behavior of cable-stayed bridges in service may be strongly affected by the time-dependent phenomena (see Bazant 1988), such as steel relaxation, in prestressed steel structures, and creep and shrinkage in concrete structures. For this reason, many authors have studied these time-dependent phenomena effects in the last decades (see Xie and Biernacki 2011). Strasky (2005) analyzed the redistribution of bending moments due to concrete time-dependent phenomena effects in a beam with vertical and inclined stays. Cluley and Shepherd (1996) analyzed the creep, shrinkage and relaxation effects in symmetric cable-stayed bridges. This analysis included the time-independent nonlinearities of large displacements in the girder and the pylon, sag effects in cable-stays and anchorage slip loss. Somja and Goyet (2008) proposed a numerical procedure for geometrical and material nonlinear finite element analysis of segmental erected structures including cable-stayed bridges. Oliveira Pedro and Reis (2010) analyzed the simulation of nonlinearities in composite steel-concrete cable-stayed bridges. Au and Si (2011) proposed a finite element analysis of the time-dependent phenomena in prestressed structures based on the time integration method. Au and Si (2012) analyzed the time-dependent effects on dynamic properties of cable-stayed bridges. In this work, the simulation of the time-dependent phenomena was carried out by mean of a time-integration method.

According to Cluley and Shepherd (1996), for a ratio of the initial prestress to the yield strength of the steel lower than 55%, steel relaxation might be neglected. This is the case of stay cables, which ratios are limited for fatigue assessment by the 45% of the ultimate strength. For this reason, in this paper only the creep and shrinkage effects are studied.

Many authors have studied the strains in concrete elements throughout time (see e.g. Barros and Martins 2012 and Ventura-Gouveia *et al.* 2011). The total strain in an axially loaded concrete element (e.g. the pylon or the deck of a cable-stayed bridge) at time  $t$  might be obtained by the superposition of elastic, thermal, shrinkage, and creep strains as follows

$$\varepsilon(t) = \varepsilon_E(t) + \varepsilon_T(t) + \varepsilon_{CS}(t, t_0) + \varepsilon_C(t, t_1) \quad (1)$$

where  $\varepsilon(t)$  is the total strain,  $\varepsilon_E(t)$  is the instantaneous Elastic strain,  $\varepsilon_T(t)$  is the Thermal strain,  $\varepsilon_{CS}(t, t_0)$  is the Shrinkage strain and  $\varepsilon_C(t, t_1)$  is the Creep strain. The first two strains of Eq. (1) can be directly calculated from the geometrical and mechanical characteristics of the structure, the concrete stresses and the environmental conditions. Nevertheless, the evaluation of  $\varepsilon_{CS}(t, t_0)$  and  $\varepsilon_C(t, t_1)$  throughout time cannot be carried out directly because both strains vary nonlinearly with time. For this reason, the simulation of the effects of creep and shrinkage phenomena requires a step by step analysis.

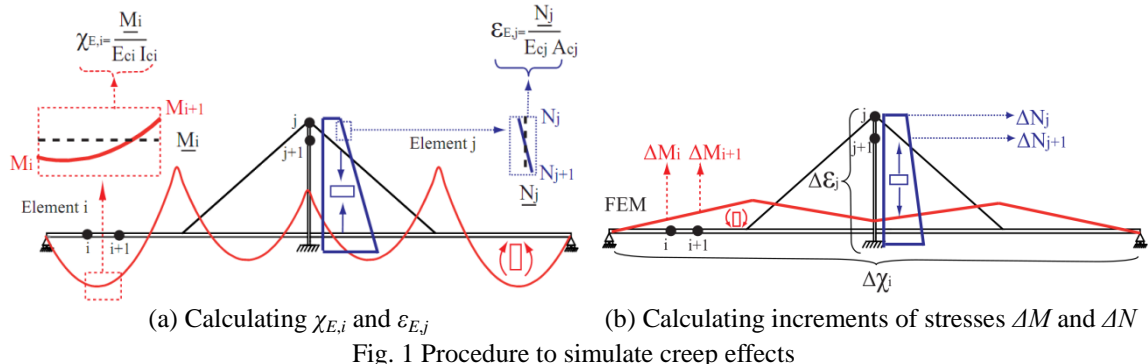


Fig. 1 Procedure to simulate creep effects

The step by step analysis to evaluate the shrinkage effects at time  $t_0 + \Delta t$  might be described as follows. Firstly, the increment of shrinkage strain,  $\Delta \epsilon_{CS,i}$ , between time  $t_0$  and  $t_0 + \Delta t$  is calculated for each  $i$ th element. These increments might be calculated as presented in Eq. (2). Secondly, these increments of strains are introduced as imposed strains in a FEM to calculate the increments of stresses due to shrinkage. Finally, to obtain the stresses at time  $t_0 + \Delta t$ , these increments of stresses are added to the stresses at time  $t_0$ . It is important to highlight, that, unlike creep, shrinkage effects do not depend on the stresses of the structure.

$$\epsilon_{CS,i} = \epsilon_{CS,i}(t + \Delta t, t_0) - \epsilon_{CS,i}(t, t_0) \quad (2)$$

The creep strain between time  $t_1$  in which a constant load is applied and evaluation time  $t$ ,  $\epsilon_C(t, t_1)$  depends linearly on the applied Elastic strain at  $t_1$ ,  $\epsilon_E(t_1)$ , as follows:

$$\epsilon_C(t, t_1) = \varphi(t - t_0, t_1 - t_0) \epsilon_E(t_1) \quad (3)$$

in which  $\varphi(t - t_0, t_1 - t_0)$  is known as the creep coefficient at time  $t$  when a load is introduced at time  $t_1$  in a concrete age  $t_0$ . Most of the methods proposed in the literature include the Dischinger's hypothesis (also known as "Rate of Creep", see Bazant 1988) to approximate the creep coefficient.

To simulate the creep effects throughout time, the procedure described in Fig. 1 might be used. This procedure is summarized as follows: (1) Firstly, the elastic curvatures,  $\chi_{E,i}$ , and the elastic strains,  $\epsilon_{E,i}$ , in every  $i$ th beam element at time  $t_0$  are calculated. For a certain stress state, these strains might be calculated from the average bending moments,  $\bar{M}_i$  and the average axial forces,  $\bar{N}_i$  in each beam element. The calculation of these average values is illustrated in Fig. 1(a). This figure includes the bending moment diagram at the deck and the axial diagram at the pylon for permanent loads. The first beam element (named beam  $i$ ) is located at the deck and their both edges are called  $i$  and  $i+1$ , respectively. If a short length of the beam  $i$  is assumed,  $\bar{M}_i$  might be approximated from the bending moments at both edges of the elements ( $M_i + M_{i+1}$ ) as presented in Eq. (4). With  $E_{c,i}$  and  $I_{c,i}$  being the Young's modulus of the  $i$ th beam element,  $\chi_{E,i}$  might be estimated from  $\bar{M}_i$  as presented in Eq. (5) and Fig. 1(a). This figure also shows the calculation of the  $\bar{N}_i$  in a  $j$ th beam element from the axial forces in both edges  $N_j$  and  $N_{j+1}$  as presented in Eq (6). With  $A_{c,i}$  being the area of the  $j$ th element,  $\epsilon_{E,i}$  might be estimated from  $\bar{N}_i$  as presented in Eq. (7) and Fig. 1(a). Once the elastic curvatures and strains are calculated, (2) the increment of curvature,  $\Delta \chi_i$  and strain,  $\Delta \epsilon_i$  in each element due to creep between time  $t_1$  and  $t_1 + \Delta t$  might be calculated. These increments are calculated as presented in Eqs. (8)-(9), where the elastic curvatures and

strains are amplified by an increment of creep factor,  $\Delta\varphi$  defined from codes. With  $\varphi(t_1 + \Delta t, t_1)$  being the creep coefficient at time and  $t_1 + \Delta t$  of a structure loaded at time  $t_1$  and  $\varphi(t_1, t_1)$  being the creep coefficient of the same structure at time  $t_1$ , the increment of creep coefficient between time  $t_1$  and  $t_1 + \Delta t$ , might be calculated as presented in Eq. (10). After calculating  $\Delta\chi_i$  and  $\Delta\varepsilon_j$ , (3) these increments might be introduced as imposed loads into the Finite Element Model (*FEM*) to calculate the increments of stresses produced by creep between time  $t_1$  and time  $t_1 + \Delta t$ . The obtained increments of bending moment,  $\Delta M$  and axial forces,  $\Delta N$ , in the edges of beam elements  $i$  and  $j$ , when  $\Delta\chi_i$  and  $\Delta\varepsilon_j$  are introduced as imposed loads are illustrated in Fig. 1(b). (4) Finally, the stresses at time  $t_1 + \Delta t$  are calculated by adding the increments of stresses produced by creep effects to the stresses at time  $t_1$ .

$$\overline{M}_i = \frac{M_i + M_{i+1}}{2} \quad (4)$$

$$\overline{x}_{E,i} = \frac{M_i}{E_{c,i} \cdot I_{c,i}} \quad (5)$$

$$\overline{N}_j = \frac{N_j + N_{j+1}}{2} \quad (6)$$

$$\overline{\varepsilon}_{E,i} = \frac{\overline{N}_j}{E_{c,i} \cdot A_{c,j}} \quad (7)$$

$$\Delta\chi_i = \chi_{E,i} \Delta\varphi(t_1 + \Delta t, t_1) \quad (8)$$

$$\Delta\varepsilon_j = \varepsilon_{E,j} \Delta\varphi(t_1 + \Delta t, t_1) \quad (9)$$

$$\Delta\varphi = \varphi(t_1 + \Delta t, t_1) - \varphi(t_1, t_1) \quad (10)$$

The increments of time used to simulate creep effects might be chosen to keep  $\Delta\varphi$  constant. In this way, these increments are selected smaller at short times and they are increased throughout time. In this paper, the formulation of the Model Code (2012) has been considered to calculate both  $\Delta\varepsilon_{CS}$  and  $\Delta\varphi$ .

## 2.2 Optimization objectives

According to the Rigidly Continuous beam Criterion (Lazar 1972) the stay cable forces in the Objective Service Stage (*OSS*), can be defined as the projections into the stay direction of the reactions of an equivalent continuous beam. This beam is obtained by substituting the stay cables by fixed supports. The  $N$  stay cable forces can be clustered into a vector,  $\{N^{OSS}\}$ . These forces can be obtained by the sum of a passive,  $\{N_P\}$ , and an active state,  $\{N_A\}$ , as presented in Eq. (11). On the one hand,  $\{N_P\}$  includes the passive stay cable forces produced when a certain Target Load,  $TL$ , is applied into the structure. On the other hand,  $\{N_A\}$  includes the effects of prestressing operations in the stay cables.

$$\{N^{OSS}\} = \{N_P\} + \{N_A\} = \{N_P\} + [\Delta N] \{\varepsilon^{OSS}\} \quad (11)$$

The forces in  $\{N_A\}$  can be simulated by introducing a set of imposed strains,  $\{\varepsilon^{OSS}\}$ , into the stay cables. These must take into account the stiffness of the whole structure. To do so, an influence matrix,  $[\Delta N]$  is required. This matrix includes the effect of the prestressing of every single stay in the rest of stays in terms of stay forces. The only unknown of Eq. (11) is  $\{\varepsilon^{OSS}\}$ , and it can be directly defined by mean of the inverse of  $[\Delta N]$ ,  $[\Delta N]^{-1}$  as presented in the following equation:

$$\{\varepsilon^{OSS}\} = [\Delta N]^{-1} (\{N^{OSS}\} - \{N_P\}) \quad (12)$$

Once calculated, the strains  $\{\varepsilon^{OSS}\}$  can be used to simulate the construction process of cable-stayed bridges as presented in Lozano-Galant *et al.* 2013. Moreover, the procedure explained in this section can be adapted to deal with the effects of the staggered erection of the superstructure of cable-stayed bridges (see Lozano-Galant *et al.* 2014). Nevertheless, up to now, this procedure has not been adapted to deal with time-dependent phenomena effects. In order to show the necessity of dealing with these effects, the following example is analyzed.

### 2.2.1 Example 1: Alamillo bridge

This example illustrates the important role of time-dependent phenomena effects in an asymmetrical concrete cable-stayed bridge without backstays. Furthermore, a parametric analysis that shows how the pylon weight and stiffness affect the creep and shrinkage effects is presented.

The analyzed structure is based on a simplified model of the Alamillo Bridge in Spain (see Casas and Aparicio 1998). This model has a 80 m long concrete deck, three stay cables arranged in harp and an inclined pylon (60 m long and 51 m high). This pylon has an inclination  $\alpha$  of 120°. The geometry of the structure is summarized in Fig. 2. In this analysis, no staggered erection of the superstructure is considered and all the stays are assumed to be prestressed in a single operation at 28 days.

To model adequately the effects of creep and shrinkage the *FEM* of the bridge includes 143 beam elements (80 are used for the deck, 60 for the pylon and 3 for the stay cables). The area, Young's modulus, and inertia, of the deck and the pylon are 1m<sup>2</sup>, 35000MPa and 1 m<sup>4</sup>, respectively. The concrete strength is 45MPa. The humidity corresponds with the 70% and the notational size of the deck and the pylon is 250 mm. The stays are characterized by an area of 0.003 m<sup>2</sup>, a Young's modulus of 195000MPa and null inertia.

The stay forces of this bridge are defined by the Rigidly Continuous Beam Criterion for a permanent load of 25 kN/m. Taking into account these forces, the weight of the pylon is calculated according to the three following criteria: (1) Criterion C-1: Equilibrium of horizontal forces in the pylon. This criterion results in a light pylon with a weight of 71.5kN/m. This weight is 2.85 times higher than that of the deck, that is to say a weight ratio of 2.85 is obtained by this criterion. (2) Criterion C-2: Null bending moment at the pylon abutment. This criterion produces a weight ratio of 3.81. Finally, (3) Criterion C-3: Minimal area of the bending moments. Application of this criterion results in a heavier pylon with a weight ratio of 4.19.

A parametric analysis is carried out to evaluate the creep and shrinkage effects. In this analysis a set of 17 different models are studied. Differences between these models refer to: (1) Criterion

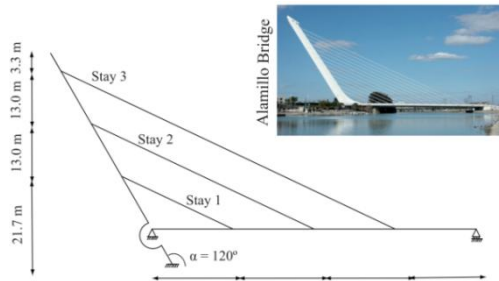


Fig. 2 Simplified model of the Alamillo Bridge (Spain)

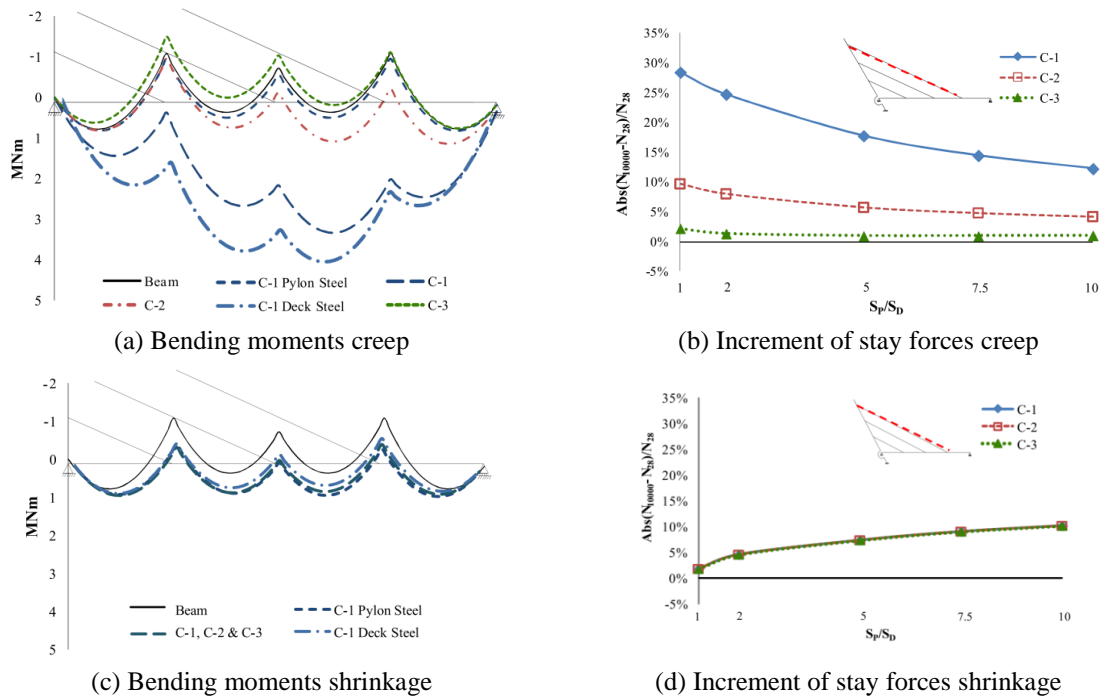


Fig. 3 Simplified model of the Alamillo Bridge (Spain)

Table 1 Imposed strains in the stays at the OSS in the models with a light pylon (C-1). The term S. Ratio indicates the stiffness ratio. The material of the deck and the pylon is also included

Model	S <sub>p</sub> /S <sub>p</sub>	Deck	Pylon	$\varepsilon_1 \cdot 10^{-3}$	$\varepsilon_2 \cdot 10^{-3}$	$\varepsilon_3 \cdot 10^{-3}$
1.1	1	Concrete	Concrete	-5.844	-5.822	-6.619
1.2	1	Steel	Concrete	-5.797	-5.783	-6.588
1.3	1	Concrete	Steel	-2.983	-2.632	-3.104
1.4	2	Concrete	Concrete	-4.101	-3.878	-4.477
1.5	5	Concrete	Concrete	-3.055	-2.712	-3.192
1.6	7.5	Concrete	Concrete	-2.822	-2.452	-2.906
1.7	10	Concrete	Concrete	-2.706	-2.323	-2.764

used to define the pylon weight (*C-1*, *C-2* or *C-3*), (2) Stiffness of the pylon. The models include a different ratio between the stiffness of the pylon ( $s_p$ ) and the stiffness of the deck ( $s_d$ ). The analyzed ratios are 1 (flexible pylon), 2, 5, 7.5 and 10 (rigid pylon). (3) Material of the deck (concrete or steel). (4) Material of the pylon (concrete or steel). For the sake of simplicity, the last two differences are only analyzed in a structure with a light (weight ratio from *C-1*) and flexible (unitary stiffness ratio) pylon.

The strains used to simulate the stay prestressing in each of the different models are calculated by the application of Eq. (12) at 28 days. As the structure is erected at that time, the calculated strains do not include the effects of the time-dependent phenomena. The obtained strains for the 7 different models with a light pylon (weight ratio from *C-1*) are summarized in Table 1. These models are named from 1.1 to 1.7. Table 1 also includes the main characteristics of the different models.

The analysis of Table 1 shows the effect of the pylon weight and stiffness in the prestressing strains. Obviously, the stiffer the pylon, the lower the prestressing strains. For example, this is appreciable by the comparison of model 1.1 (with a stiffness ratio of 1) and 1.4 (with a stiffness ratio of 2). In this case, double inertia of the pylon reduces the strains of the stay cables 29.8, 33.3 and 32.4 %, respectively. The comparison of the obtained strains in models based on *C-1*, *C-2* and *C-3* shows that the heavier the pylon, the lower the prestressing strains.

Once the structure has achieved the *OSS* at 28 days, the effects of the time-dependent phenomena in concrete at 10000 days are simulated. For each of the analyzed models, the creep and shrinkage effects are studied separately. In the analysis of each of these phenomena, the deck bending moment diagrams are used to evaluate the effects of the pylon weight as well as the different materials of the deck and the pylon (Figs. 3(a)-(c)). The effects of the pylon stiffness are evaluated by mean of the changes in the stay force with time for each pylon weight criterion (Figs. 3(b)-(d)).

The bending moment diagram in the deck obtained after adding the creep effects are summarized in Fig. 3(a). This figure includes the bending moment diagram of the *OSS* at 28 days (that corresponds with that of a continuous beam), the bending moments diagram obtained by each pylon weight criterion (*C-1*, *C-2* and *C-3*) with a unitary stiffness ratio and the bending moment diagram obtained when the pylon and the deck material is changed to steel in *C-1* with a unitary stiffness ratio. In the figure, the latter two stages are named "*C-1 Pylon Steel*" and "*C-1 Deck Steel*", respectively. The analysis of Fig 3(a) shows the following conclusions: (1) The stress redistribution due to creep at the pylon is of primary importance. This is appreciable by the comparison of the results obtained by models with different materials (*C-1 Pylon Steel*, *C-1 Deck Steel* and *C-1*). When the pylon is made of steel (*C-1 Pylon Steel*), the maximum creep redistribution (154.37kNm) only represents the 14.41% of the maximum bending moment in the *OSS* (-1.11MNm). This value is found at the mid span and it is caused by axial creep shortening of the deck. In those cases where the pylon is made of concrete (*C-1 Deck Steel* and *C-1*) the redistribution of stresses due to creep is significantly higher. The maximum redistribution in *C-1* (3091.76kNm) is found at the anchorage of the third stay and it represents the 288.56% of the maximum bending moment in the *OSS*. In the case of *C-1 Deck Steel* the maximum redistribution (3970.78kNm) is found at the mid span and it represents the 376.91% of the maximum bending moment in the *OSS*. It is important to highlight that in those cases where the pylon is made of concrete, the creep redistribution of the structure also produce changes in the sign of the bending moments of the deck (e.g. at the stay anchorage the hogging moments are changed to sagging

ones). These changes are mainly caused by the stress redistribution of the light pylon, which is subjected to high stresses at 28 days. (2) The favorable effect of the redistribution of stresses due to creep when the deck is made of concrete. This is appreciable by comparing the results of *C-1 Deck Steel* and *C-1*. In the latter case, redistribution of stresses at the deck reduces the effects of the redistribution of stresses at the pylon. (3) It is convenient to reduce the stresses of the pylon at the *OSS* to minimize its redistribution throughout time. This can be carried out by using heavier pylons as shows the comparison between models *C-1*, *C-2* and *C-3*. In *C-2* the maximum redistribution (863.09kNm) is found at the anchorage of the third stay and it represents the 80.55% of the maximum moment in the *OSS*, while in *C-3*, the maximum redistribution (414.00kNm) is found at the anchorage of the first stay and it represents the 38.17% of the maximum moment in the *OSS*.

A parametric analysis is also presented to illustrate how the pylon stiffness influences the stress redistribution due to creep phenomenon. This analysis is summarized in Fig. 3(b) in terms of the absolute percentage of variation of the axial force of the third stay between 28,  $N_{28}$ , and 10000,  $N_{10000}$ , days. The analysis of this figure shows an additional conclusion: As expected, (4) the stiffness of the pylon produces a favorable effect into the stress redistribution due to creep in all the criteria. Nevertheless, increasing the stiffness might not be enough to minimize the redistribution of stresses due to creep. This is appreciable by the comparison of the results obtained by *C-1* and *C-2*. For a unitary stiffness ratio, the variations of the stay forces throughout time represent a 28.37% (*C-1*) and a 9.68% (*C-2*) of the stay force at 28 days. When the stiffness ratio is increased to 10, these percentages are reduced to 12.23% (*C-1*) and 4.21% (*C-2*). This analysis shows again the important role of the pylon weight in the stress redistribution due to creep. When this weight is calculated to minimize the bending area of the pylon (*C-3*), the variation of the stay force in the third stay throughout time varies from 2.20% (stiffness ratio=1) to 0.97% (stiffness ratio=10). These values are significantly lower than those obtained by the rest of criteria. Placing a backstay produces a similar favorable effect that using the heavy pylon proposed in *C-3*.

The bending moments obtained in the deck after adding the shrinkage effects are presented in Fig. 3(c). The analysis of this figure shows the following conclusions: (1) The shrinkage does not depend on the stresses that the pylon is subjected to. This is appreciable by the fact that the same bending moments are obtained for the different analyzed pylon weights (*C-1*, *C-2* and *C-3*). In these models, the maximum differences with the bending moments of the equivalent continuous beam (559.01 kNm) are found at the mid span. This value represents a deviation of the 52.18% of the maximum bending moment in the continuous beam. (2) The shrinkage phenomenon depends on the materials of the bridge. This is appreciable by comparison of the bending moment diagrams of the *C-1*, *C-1 Pylon Steel* and *C-1 Deck Steel*. Nevertheless, the effects of changing the deck or the pylon material are not as significant as in the creep redistribution of stresses.

The parametric analysis that shows the effect of pylon stiffness on the stress redistribution due to shrinkage is summarized in Fig. 3(d). This figure includes the variation of the stay force in the third stay throughout time for different stiffness ratios. The analysis of Fig. 3(d) shows that, (3) Independently of the pylon weight, the pylon stiffness increases the perceptual difference with the stay force in the *OSS*. For example, the differences obtained for a unitary stiffness ratio, (2.07%) are increased to 9.08% for a stiffness ratio of 10.

This example illustrates the necessity of including the time-dependent phenomena effects into the definition of the *OSS*. To fill this gap, a new criterion is proposed in the following section.

### 3. New method to include time-dependent phenomena effects into the OSS

When time-dependent phenomena are included into the simulation of the OSS, Eq. (12) cannot be directly applied to calculate the  $\{\varepsilon^{OSS}\}$  because of the nonlinear effects produced by the time-dependent phenomena. These effects depend, to a great extent, on the structural system in which the different loads are applied. Furthermore, it is important to highlight that the OSS is only achieved at a certain Target time  $t_T$ . To solve all these problems, Eq. (11) might be rewritten as

$$\{N^{OSS,t_T}\} = \{N^{K-N,t_T}\} + \{N^{N,t_T}\} = \{N^{K-N,t_T}\} + [\Delta N^{N,t_T}] \{\varepsilon^t\} \quad (13)$$

in which the stay cable forces at  $t_T$ ,  $\{N^{OSS,t_T}\}$ , obtained by the sum of two different vectors of stay forces  $\{N^{K-N,t_T}\}$ , and  $\{N^{N,t_T}\}$ . With  $K$  being the number of construction stages and  $N$  being the number of stays, the former of these vectors represents the stay cable forces after the first  $K-N$  tensioning operations. In these stages changes in the structural system are simulated both during the staggered erection of the superstructure and during the prestressing of the stay cable system. These forces include the effects of the time-dependent phenomena from the beginning of the staggered erection of the superstructure until  $t_T$ . The effect of the application of the remaining of the permanent loads at time  $t_{PL}$  might also be introduced into the simulation of the stay forces of this vector. On the other hand, the vector  $\{N^{K-N,t_T}\}$  represents the stay forces in the last  $N$  tensioning operations (last re-tensioning operation) after including the time-dependent phenomena at time  $t_T$ . As in common practice, the structural system in these operations is assumed to correspond with that of the complete structure (with all stay cables and no temporary supports). The vector  $\{N^{K-N,t_T}\}$  might be expressed as the sum of an influence matrix in terms of increments of stay forces,  $[\Delta N^{N,t_T}]$ , and a vector of imposed strains,  $\{\varepsilon^t\}$ . This vector  $\{\varepsilon^t\}$  represents the strains to be introduced into the last tensioning operation of each stay at their respective prestressing times.

If the stay cables are installed in two tensioning operations, that is to say,  $K=2N$ , Eq. (13) might be developed as presented in Eq. (14). The time of each tensioning operations is named  $t_{k,m}$ . The first sub-index refers to the prestressed stay and the second one to the number of its tensioning operation. For example,  $t_{1,2}$  indicates the time in which the second tensioning operation of the first stay is carried out. The sub-indices in vectors  $\{N^{OSS}\}$  and  $\{N^{K-N,t_T}\}$  refer to each of the stay cables. For example, the stay forces in the OSS in the  $n$ th stay is called  $N_n^{OSS,t_T}$ . Each  $n$ th column of matrix  $[\Delta N^{N,t_T}]$  corresponds with the forces in all stay cables at time  $t_T$  when a unitary strain,  $\varepsilon_n^{t_{n,2}}$ , is introduced in the last tensioning operation of the  $n$ th stay at time  $t_{n,2}$ . The nomenclature used in each of the terms of this matrix is as follows: the first super-index corresponds with the construction stage in which the  $n$ th stay is re-stressed, the second super-index refers to the evaluation time,  $t_T$ , the first sub-index corresponds with the unitary strain introduced in the stay at the time of the re-stressing operation  $t_{n,2}$ , and the second sub-index refers to the stay in which the increment of stay force is calculated. The vector  $\{\varepsilon^t\}$  is divided into the imposed strains to be introduced into each stay  $n$  in its last tensioning operation at time  $t_{n,2}$ .

$$\begin{bmatrix} N_1^{OSS,t_T} \\ \vdots \\ N_n^{OSS,t_T} \\ \vdots \\ N_N^{OSS,t_T} \end{bmatrix} = \begin{bmatrix} N_1^{K-N,t_T} \\ \vdots \\ N_n^{K-N,t_T} \\ \vdots \\ N_N^{K-N,t_T} \end{bmatrix} + \begin{bmatrix} \Delta N_{\varepsilon_1^{t_{1,2},1}}^{K-N+1,t_T} & \dots & \Delta N_{\varepsilon_n^{t_{n,2},1}}^{K-N+n,t_T} & \dots & \Delta N_{\varepsilon_N^{t_{N,2},1}}^{K,t_T} \\ \vdots & & \vdots & & \vdots \\ \Delta N_{\varepsilon_1^{t_{1,2},n}}^{K-N+1,t_T} & \dots & \Delta N_{\varepsilon_n^{t_{n,2},n}}^{K-N+n,t_T} & \dots & \Delta N_{\varepsilon_N^{t_{N,2},n}}^{K,t_T} \\ \vdots & & \vdots & & \vdots \\ \Delta N_{\varepsilon_1^{t_{1,2},N}}^{K-N+1,t_T} & \dots & \Delta N_{\varepsilon_n^{t_{n,2},N}}^{K-N+n,t_T} & \dots & \Delta N_{\varepsilon_N^{t_{N,2},N}}^{K,t_T} \end{bmatrix} \begin{bmatrix} \varepsilon_1^{t_{1,2}} \\ \vdots \\ \varepsilon_n^{t_{n,2}} \\ \vdots \\ \varepsilon_N^{t_{N,2}} \end{bmatrix} \quad (14)$$

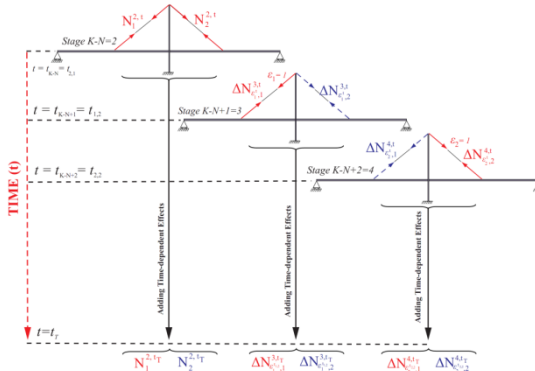


Fig. 4 Definition of stay forces in  $\{N^{K-N, tT}\}$  and in  $[\Delta N^{N, tT}]$  for a 2-stay cable-stayed bridge

To illustrate the different terms of Eq. (14), this equation is applied to a two-stay cable-stayed bridge as presented in Eq. (15). The tensioning process of this structure includes four tensioning operations. In the first two operations the two stays are placed at times  $t_{1,1}$  and  $t_{2,1}$ , while in the last two tensioning operations the stay forces are adjusted at times  $t_{1,2}$  and  $t_{2,2}$ . In this case, the stay cable forces in the OSS of every stay, that is to say,  $N_1^{OSS,tT}$  and  $N_2^{OSS,tT}$ , might be calculated by projecting the reactions of an equivalent continuous beam into the stay cable directions. The stay forces after the first two tensioning operations (first  $K-N=2$  tensioning operations) at time  $t_T$ ,  $N_1^{2,tT}$  and  $N_2^{2,tT}$ , are obtained when the effects of the time-dependent phenomena are added to the results of the first tensioning operation. The calculation of the terms of the stay forces after the first  $K-N$  tensioning operations at time  $t_T$  is summarized in Fig. 4.

$$\begin{Bmatrix} N_1^{OSS,tT} \\ N_2^{OSS,tT} \end{Bmatrix} = \begin{Bmatrix} N_1^{2,tT} \\ N_2^{2,tT} \end{Bmatrix} + \begin{bmatrix} \Delta N_{\varepsilon_1^{t_{1,2},1}}^{3,tT} & \Delta N_{\varepsilon_2^{t_{2,2},1}}^{4,tT} \\ \Delta N_{\varepsilon_1^{t_{1,2},2}}^{3,tT} & \Delta N_{\varepsilon_2^{t_{2,2},2}}^{4,tT} \end{bmatrix} \begin{Bmatrix} \varepsilon_1^{t_{1,2}} \\ \varepsilon_2^{t_{2,2}} \end{Bmatrix} \quad (15)$$

In Eq. (15), the forces in  $[\Delta N^{N,tT}]$  include the effects of the last  $N = 2$  tensioning operations. Terms of each column of this matrix represents the last  $N$  tensioning operations. The first column corresponds with the first re-tensioning operation (Stage 3 at time  $t_{1,2}$ ), while the second one corresponds with the second re-tensioning operation (Stage 4 at time  $t_{2,2}$ ). Each of these operations is simulated by mean of an independent FEM as presented in Fig. 4. The FEM of the first column of  $[\Delta N^{N,tT}]$  includes the increments of stay forces produced by a unitary strain applied at the first stay cable at time  $t_{1,2}$ . This strain produces some active forces (highlighted in red) in the first stay and some passive forces (highlighted in discontinuous blue) in the second stay cable. Then, the creep effects produced until  $t_T$  are introduced. The FEM of the second column includes an imposed strain at the second stay cable. The increment of forces of this tensioning operation only include the effects of the time-dependent phenomena from time  $t_{2,2}$  to  $t_T$  as presented in Fig. 4.

The only unknown of Eq. (13) is the vector of imposed strains  $\{\varepsilon^t\}$ . This vector might be obtained by mean of the inverse of the influence matrix of stay forces  $[\Delta N^{N,tT}]^{-1}$  as follows

$$\{\varepsilon^t\} = [\Delta N^{N,tT}]^{-1} (\{N^{OSS,tT}\} + \{N^{K-N,tT}\}) \quad (16)$$

The set of strains in vector  $\{\varepsilon^t\}$  might be used to simulate the effects of the time-dependent phenomena into the *OSS*. For example, the bending moments at time  $t_T$ ,  $\{M^{OSS,t}\}_T$  might be simulated by the following equation

$$\{M^{OSS,t_T}\} = \{M^{K-N,t_T}\} + [\Delta M^{N,t_T}] \{\varepsilon^t\} \quad (17)$$

in which  $\{M^{K-N,t_T}\}$  is a vector that includes the bending moments after including the effects of the time-dependent phenomena into the last  $K-N$  stages at time  $t_T$  and  $[\Delta M^{N,t_T}]$  is an influence matrix that includes the bending moments in the last  $N$  tensioning operations when a unitary strain is introduced into each stay and after adding the effects of the time-dependent phenomena at time  $t_T$ .

#### 4. Application of the new method

In this section two structures (Example 2 and Example 3) are analyzed by the method presented in the preceding section. On the one hand, in Example 2 the method is applied to assure the achievement of the *OSS* in 10000 days. Furthermore, the effects of the pylon stiffness are also analyzed. On the other hand, in Example 3 the strains in the *OSS* are defined for two different criteria ( $OSS_{130}$  and  $OSS_{10000}$ ). Differences between these criteria refer to the target time (130 and 10000 days, respectively) in which the *OSS* is defined to be achieved.

In Examples 2 and 3, the staggered erection of the superstructure and the tensioning operations of the stay cables are not considered. That is to say, it has been assumed that the structure is erected in a single operation at 28 days.

##### 4.1 Example 2: Alamillo bridge

The mechanical and geometrical characteristics of this structure correspond with those presented in Example 1, for a unitary stiffness ratio between the pylon and the deck. As in the pointed example, the pylon weight is defined by different criteria (C-1, C-2 and C-3). The model obtained for each of the three different pylon weights are named from 2.1 to 2.3. The *OSS* of each of the models might be characterized by a set of imposed strains  $\{\varepsilon^t\}$ . These strains have been calculated to assure the achievement of the *OSS* at 10000 days. The calculation of these strains has been carried out by Eq. (16).

The main characteristics and the obtained strains for each of the analyzed models are summarized in Table 2. The analysis of this table indicates that the heavier the pylon, the lower the required strains. For example, the average strain in the model with a light pylon (model 2.1) is 8.98 times higher than the average strain in the model with a heavy pylon (model 2.3).

Table 2 Strains in the different stays

Model	Pylon weight	S.Ratio	$\varepsilon_1 \cdot 10^{-3}$	$\varepsilon_2 \cdot 10^{-3}$	$\varepsilon_3 \cdot 10^{-3}$
2.1	C-1	1	-15.514	-16.181	-17.527
2.2	C-2	1	-5.634	-5.747	-6.651
2.3	C-3	1	-1.681	-1.571	-2.230

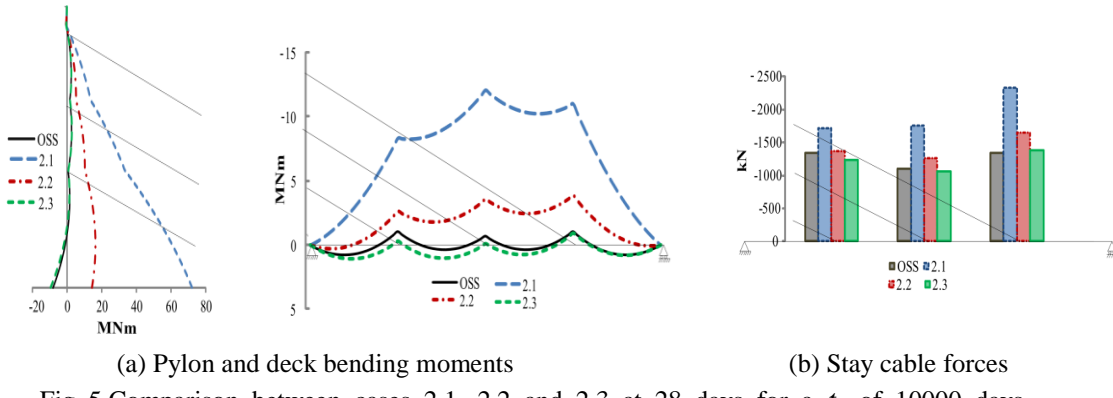


Fig. 5 Comparison between cases 2.1, 2.2 and 2.3 at 28 days for a  $t_T$  of 10000 days

The different strains presented in Table 2 might be used to simulate the stresses of the structure at any time. For example, the bending moments might be calculated by application of Eq. (16).

The pylon and deck bending moment diagrams at 28 days obtained for the different cases are presented in Fig. 5(a). These bending moment diagrams are also compared with those obtained at 10000 days at the OSS (minimal bending energy). The analysis of this figure shows that the lighter the pylon, the higher the value of bending moments required at 28 days to assure the achievement of the OSS at 10000 days. This is appreciable by comparing the maximum differences of the bending moments between 28 and 10000 day obtained by models 2.1 and 2.3. In the case 2.1, the maximum differences at the deck (11.01MNm) are 9.90 times the maximum bending moment in the OSS (-1.11MNm). These differences are reduced to 0.79MNm in model 2.3. This value represents 71.2% of the maximum bending moment at the OSS.

The stay forces in each of the analyzed cases at 28 days are presented in Fig. 5(b). This figure also includes the stay forces in the *OSS*. The analysis of this figure shows similar results than those obtained by the analysis of the bending moment diagrams. The higher differences are found in case 2.1 in which the maximum stay force (-2330.82kN) represents a deviation of the 73.79% of the corresponding force in the *OSS*. On the contrary the maximum differences at the first stay in case 2.3 (-1236.68kN) represents a deviation of the 8.15% of the stay force in the *OSS*.

Fig. 5 illustrates the important role that the pylon plays in the redistribution of stresses due to the time-dependent phenomena effects. In this kind of structures it is convenient to define the weight of the pylon by minimizing the area of the pylon bending moment diagram (criterion C-3). In this case, the variation of the structural behavior throughout time due to time-dependent phenomena effects is reduced when compared with the other analyzed criteria.

## 4.2 Example 3: Wuxi bridge

The cable-stayed bridge analyzed in this section is presented in Fig. 6 and corresponds with a simplified model of a project for the city of Wuxi in China. The model has a concrete pylon 55m high, a 180m long concrete deck and  $N = 19$  stay cables arranged in a fan symmetric form. The self weight of the bridge deck,  $g_1$ , and the target load,  $TL$ , are 135kN/m and 202.5kN/m,

respectively. The stay cables are uniformly anchored every 9 m along the deck. In service the structure includes a live load of 40 kN/m.

The *FEM* of the whole bridge includes 489 beam elements (360 for the deck, 110 for the pylon and 19 for the stays). The area, Young's modulus and inertia of the deck are  $5.4 \text{ m}^2$ , 33500MPa and  $4.2 \text{ m}^4$ , respectively. The mechanical properties of the pylon are  $8.54 \text{ m}^2$ , 33500MPa and  $14.4 \text{ m}^4$ . The concrete strength is 45MPa, the relative humidity is 70% and the notional size of the deck and the pylon is 500 and 1900 mm, respectively. The stays have an area of  $0.0072 \text{ m}^2$ , a Young's modulus of 195000MPa and null inertia.

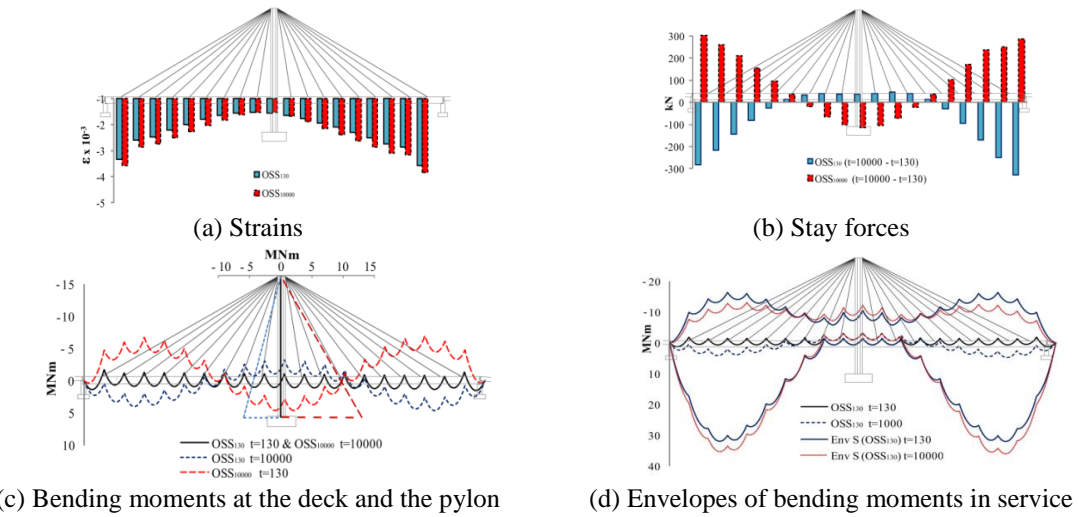
Two different criteria are used to define the prestressing strains in the *OSS*. The first criterion,  $OSS_{130}$ , defines these strains to achieve the *OSS* at 130 days while the second criterion,  $OSS_{10000}$ , defines these strains to achieve the *OSS* at 10000 days.

Application of Eq. (15) provides the strains summarized in Fig. 7(a). In the  $OSS_{130}$  the strains vary from  $-1.511 \cdot 10^{-3}$  at the central stay to  $-3.576 \cdot 10^{-3}$  at the edged stays. These strains are increased to  $-1.516 \cdot 10^{-3}$  at the central stay and to  $-3.842 \cdot 10^{-3}$  in the criterion  $OSS_{10000}$ . The maximum differences between strains of both cases are found in the 15<sup>th</sup> stay ( $C_{15}$ ). The strain of this stay in  $OSS_{10000}$ ,  $-2.634 \cdot 10^{-3}$ , is 14.71% higher than that obtained by  $OSS_{130}$ .

The creep and shrinkage effects produce changes in the forces of the stays due to permanent loads in service. This is appreciable in Fig. 7(b), where the differences in stay forces between 130 and 10000 days are presented for the two criteria. The analysis of this figure shows that in the  $OSS_{130}$  stay forces in the proximities of abutments are reduced with time. The maximum reduction (327.25kN) is found at  $C_{19}$  and it represents a 6.91% of its stay force in the *OSS*. In the proximities of the pylon, stay forces are increased. The maximum increase (45.84kN) is found in  $C_{12}$ . This value represents the 2.91% of its stay force in the *OSS*. The effects throughout time when the stay forces are defined by  $OSS_{10000}$  are the opposite ones. This means that the stays in the proximities of the abutments increase its force with time and the stays in the proximities of the pylon reduce its force with time.

The pylon and deck bending moment diagrams for permanent loads obtained by both criteria at 130 and 10000 days are presented in Fig. 7(c). In the  $OSS_{130}$  criterion, the bending moment diagram of the equivalent continuous beam (with maximum sagging and hogging moments of 1293.96 and -1758.58kNm at deck, respectively) is achieved at 130 days. At this time no bending moments appear at the pylon. Then, creep and shrinkage effects modify successively bending diagrams and at 10000 days the maximum sagging and hogging moments are increased to 4603.66 and -3178.85kNm in the deck and to -6006.30kNm in the pylon. In the  $OSS_{10000}$  criterion, the continuous beam behavior is achieved at the deck at 10000 days. In this case the maximum sagging and hogging moments (with a value of 4479.94 and -6679.11kNm, respectively at the deck and 12911.08kNm at the pylon) are achieved at 130 days. Analysis of these results shows that higher changes in the bending moment diagram throughout time are produced when the strains are defined to achieve the *OSS* at 10000 days ( $OSS_{10000}$  criterion).

The Envelopes in Service (*EnvS*) of the deck bending moment diagrams at 130 and 10000 days obtained by  $OSS_{130}$  are presented in Fig. 7(d). This figure also includes the bending moment diagrams for permanent loads at 130 and 10000 days. This figure shows that the creep and shrinkage effects increase the sagging bending moments in the proximities of the abutments. These increments produce unfavorable effects in the minimum envelope of negative bending moments, in which the maximum differences (-4065.51kNm) throughout time are found between the 17<sup>th</sup> and

Fig. 7 Simulation of time-dependent phenomena effects of  $OSS_{130}$  and  $OSS_{1000}$ 

the 18<sup>th</sup> stay anchorages. It is important to notice that in structures suspended on multiple stay cables, the bending moments due to the dead load are very small compared to those produced by live load (see Strasky 2005). In fact, these differences represent a 292.89% of the maximum bending moment of the OSS and only the 11.31% of the maximum sagging moment of the envelope.

## 5. Conclusions

This paper studies the creep and shrinkage effects in service stresses of concrete cable-stayed bridges. To illustrate the importance of these phenomena, a parametric analysis of an asymmetrical cable-stayed bridge without backstay is presented. In this analysis the influence of the pylon weight and stiffness is analyzed. This analysis shows that in this kind of structures, creep of the pylon is the phenomenon that produces the greater effects in service. Furthermore, pylon weight proved to be of primary importance to reduce the creep redistribution of stresses. To minimize this redistribution, the pylon weight must minimize the bending area of the pylon in the Objective Service Stage (OSS). Despite the fact that the pylon stiffness presents a favorable effect, this might not be enough to minimize the redistribution of stresses due to creep in light pylons. In these cases, the placement of a backstay is advised. Due to the large bending moments that the pylon is subjected to, in the analyzed example shrinkage effects are lower in magnitude than creep effects. Regarding this phenomenon, the same results are obtained independently of the pylon weight.

Despite of its importance, most of the criteria presented in the literature to define the OSS do not include the time-dependent phenomena effects. To fill this gap, a new method has been proposed to include these effects into the definition of the OSS. To illustrate the application of this method, two structures were analyzed. The first structure (Example 2) shows that in asymmetrical bridges without backstay is not adequate to define the OSS to be achieved when the time-dependent phenomena effects have been completely developed because large stresses are obtained

in early times. This is especially problematic in structures with flexible pylons. This example also shows that when the pylon weight is defined to minimize the area of the pylon bending moment diagram, the structural response in service is significantly improved as it remains practically constant in time. The analysis of the second structure (Example 3) also recommended the definition of the OSS in early times.

## Acknowledgments

The authors wish to thank the Ministerio de Ciencia e Innovación and the Junta de Comunidades de Castilla-La Mancha (Spain) for the financial support through the research Projects BIA2009-13056 and PII2I09-0129-4085 (Optimization of the construction process of cable-stayed bridges built on temporary supports), directed by José Turmo.

## References

- Au, F.T.K. and Si. X.T. (2011), "Accurate time-dependent analysis of concrete bridges considering concrete creep, concrete shrinkage and cable relaxation", *Eng. Struct.*, **33**(1), 118-126.
- Au, F.T.K. and Si. X.T. (2012), "Time dependent effects on dynamic properties of cable-stayed bridges". *Struct. Eng. Mech.*, **41**(1), 139-155.
- Barros, H.F.M. and Martins, R.A.F. (2012), "Nonlinear analysis of service stresses in reinforced concrete sections-closed form solutions", *Comput. Concrete*, **10**(5), 541-555.
- Bazant, Z. (1998), *Mathematical Modeling of Creep and Shrinkage of Concrete*, John Wiley & Sons Ltd.
- Casas, J.R. and Aparicio. A.C. (1998), "Monitoring of the Alamillo cable-stayed bridge during construction", *Exper. Mech.*, **38**(1), 24-28.
- Chen, D.W. Au, F.T.K. Tham, L.G. and Lee, P.K.K. (2000), "Determination of initial cable forces in prestressed concrete cable-stayed bridge for given design deck profiles using the force equilibrium method", *Comput. Struct.*, **74**(1), 1-9.
- Cluley, N.C. and Shepherd, R. (1996), "Analysis of concrete cable-stayed bridges for creep, shrinkage and relaxations effects", *Comput. Struct.*, **58**(2), 337-350.
- Du, G.H. (1989), "Optimal cable tension and construction tensioning of cable-stayed bridges", *Bridge Construct.*, **74**, 18-22.
- Fiore, A., Monaco, P. and Raffaele, D. (2012), "Viscoelastic behavior of non-homogeneous variable-section beams with post-poled restraints", *Comput. Concrete*, **9**(5), 357-374.
- Gimsing, N.J. (1997), *Cable Supported Bridges, Concept and Design*, John Wiley and Sons, Chichester.
- Giussani, F., Minoretti, A., Mola, F. and Savoldi, C. (2004), Improvements in long term structural analysis of cable-stayed bridges, Conference on our World in Concrete and Structures, Singapore, 25-26, August. 29th.
- Gocic, M. and Sadovic, E. (2012), "Software for application of Newton-Raphson method in estimation of strains in prestressed concrete girders", *Comput. Concrete*, **10**(2) 121-131.
- Guan, H. (2000), "Construction Control of Cable-Stayed Bridges", Ph.D. Dissertation, The Hong Kong University of Science and Technology, Hong Kong.
- Hassan, M.M. Nassem, A.O. and El Damatty A.A. (2012), "Determination of optimum post-tensioning cable forces of cable-stayed bridges", *Eng. Struct.*, **44**, 248-259.
- Hassan, M.M. (2013), "Optimization of stay cables in cable-stayed bridges using finite element, genetic algorithm, and B-spline combined technique", *Eng. Struct.*, **49**, 643-654.
- Janjic, D. Pircher, M. and Pircher, H. (2002), "The unit load method - some recent applications", *Adv. Steel Struct.*, I-II: 831-837.

- Janjic, D. Pircher, M. and Pircher, H. (2003), "Optimization of cable-tensioning in cable-stayed bridges", *J. Bridge Eng.*, **8**, 131-137.
- Lazar, B.E. Troitsky, M.S. and Douglas, M.C. (1972), "Load analysis balancing of cable stayed bridges", *ASCE J. Struct. Eng.*, **92**(8), 1725-1740.
- Lozano-Galant, J.A. Payá-Zaforteza, I. Xu, D. and Turmo J. (2012), "Analysis of the construction process of cable-stayed bridges built on temporary supports", *Eng. Struct.*, **40**, 95-106.
- Lozano-Galant, J.A. Payá-Zaforteza, I. Xu, D. and Turmo J. (2012), "Forward algorithm for the construction control of cable-stayed bridges built on temporary supports", *Eng. Struct.*, **40**, 119-130.
- Lozano-Galant, J.A. Xu, D. Payá-Zaforteza, I. and Turmo J. (2013), "Direct simulation of the tensioning process of cable-stayed bridges", *Comput. Struct.*, **121**, 119-130.
- Lozano-Galant, J.A., Ruiz-Ripoll, L., Payá-Zaforteza, I. and Turmo, J. (2014), "Modification of the stress-state of cable-stayed bridge due to staggered erection of their superstructure", *Baltic J. Road Bridge Eng.*, In press.
- Martins, A.M.B. Simoes, L.M.C. and Negrao, J.H.O. (2011), Time-dependent analysis and cable stretching force optimization of concrete cable-stayed bridges, International Conference on Recent Advantages in Nonlinear Models Structural Concrete Application, CoRAN2011, 24-25 November, Coimbra, Portugal.
- Model code (2012), fib Bulletin No. 65. Model Code 2010 - Final draft, Volume 1.
- Negrao, J.H.O. and Simoes, L.M.C. (1997), "Optimization of cable-stayed bridges with three dimensional modeling", *Comput. Struct.*, **64**(1-4), 741-758.
- Strasky, J. (2005), *Stress Ribbon and Cable-Supported Pedestrian Bridges*. Thomas Telford, London.
- Oliveira Pedro, J.J. and Reis, A.J. (2010), "Nonlinear analysis of composite steel-concrete cable-stayed bridges", *Eng. Struct.*, **32**, 2702-2716.
- Scotti, A. (2003), "Long term behavior of cable-stayed bridges", Master thesis Dissertation, Politecnico di Milano, Italy.
- S.E.T.R.A. (2001). "Haubans. Recommandations de la Commission Interministérielle de la Précontrainte", Service d'Etudes Techniques des Routes et Autoroutes, France.
- Simoes L.M.C. and Negrao, J.H.O. (2000), "Optimization of cable-stayed bridges with box-girder decks", *Adv. Eng. Softw.*, **31**, 417-423.
- Somja, H. and de Goyet, V. (2008), "A new strategy for analysis of erection stages including an efficient method for creep analysis", *Eng. Struct.*, **30**, 2871-2883.
- Ventura-Gouveia, A., Barros, J.A.O. and Azevedo, A.F.M. (2011), "Crack constitutive model for the prediction of punching failure modes of fiber reinforced concrete laminar structures", *Comput. Concrete*, **8**(6), 735-755.
- Wang, P.H. Tseng, T.C. and Yang, C.G. (1993), "Initial shape of cable-stayed bridges", *Comput. Struct.*, **46**(6), 1095-1106.
- Xie, T. and Biernacki, J.J. (2011), "The origins and evolution of cement hydration models", *Comput. Concrete*, **8**(6), 647-675.